







# Spatial Iterative Learning Torque Control of Robotic Exoskeletons for High Accuracy and Rapid Convergence Assistance

Xueyan Xing , Member, IEEE, Sainan Zhang , Tzuhao Huang , Jin Sen Huang , Hao Su , Senior Member, IEEE, and Yanan Li , Senior Member, IEEE

**Abstract**—High-performance torque tracking is crucial for accurate control of the magnitude and timing of exoskeleton assistive torque profiles. However, state-of-the-art torque control methods, e.g., iterative learning control (ILC), applied to exoskeletons cannot achieve satisfying accuracy and convergence speed. This article aims to design a spatial iterative learning (sIL)-based torque control strategy for exoskeletons to achieve accurate and fast torque assistance, which includes a high-level controller for torque planning, a mid-level one for reference trajectory generation, and a low-level one for trajectory tracking. Compared with ILC, our proposed sIL-based control method can estimate and compensate for spatial uncertainties (e.g., joint-angle-related uncertain dynamics of the human-exoskeleton interaction system) and spatial disturbances (e.g., joint-angle-related disturbances caused by physical interaction with the human limb) that commonly exist in exoskeletons for highly accurate torque assistance. Furthermore, our control can ensure accurate torque tracking during unsteady-state gaits with fast convergence thanks to its spatial learning capability that enables varying iterative learning speeds to deal with varying walking speeds of users for different iterations, which is not feasible by ILC methods. Experiments showed that compared with the state-of-the-art torque control methods, our sIL-based control method significantly improved the torque tracking accuracy and shortened the convergence time for

both steady-state walking and unsteady-state walking (with sudden or gradual changes in gait speeds), which demonstrates its effectiveness.

**Index Terms**—Exoskeleton, human-robot interaction, robustness, spatial iterative learning control.

## I. INTRODUCTION

ASSISTIVE lower-limb exoskeletons such as ankle, knee, and hip exoskeletons have great potential to restore and augment human mobility [1], [2], [3]. To maximize the potential, assistive exoskeletons are required to minimize resistance to users' volitional motion, which means appropriate assistive torque reference and accurate torque delivery are necessary. In terms of the magnitude of assistive torque, excessive torque tracking error leads to instability, thus minimizing the error is necessary [4]. The timing of assistive torque also has a significant influence on the benefits of exoskeletons. A 2.5% delay can offset all the benefits of exoskeletons and increase the energy penalty [5], [6]. Therefore, torque controller design is one of the most important aspects of improving the performance of wearable robots.

Control of exoskeletons is typically hierarchical, including high-level and low-level control. In comparison, the low-level control achieves assistive torque according to the torque reference from high-level control [7], [8], [9]. In torque-controlled human-exoskeleton interactive systems, torque tracking accuracy is equivalent to the precision of the assisted motion and, thus, directly affects the assistance performance [10], maximizing exoskeleton's potential hinges on the simultaneous effectiveness of high-level and low-level control mechanisms. However, there is still a lack of research that aims at designing a multilevel controller to make the low-level controller effectively cooperate with the high-level controller for torque assistance with high accuracy.

Low-level controllers, namely torque control, of lower-limb exoskeletons can be classified into classical feedback control [11], model-based control [12], adaptive control [13], and time-based iterative learning control (ILC) [14]. Classical feedback control [11] is a simple method but with limited robustness, which makes the control accuracy easily affected by the disturbance. Model-based control [12] improves tracking accuracy but demands a precise dynamic model, which is neither easy to

Manuscript received 14 September 2023; revised 28 January 2024; accepted 3 February 2024. Recommended by Technical Editor S. Chen and Senior Editor K. J. Kyriakopoulos. The work of X. Xing and Y. Li was supported by the U.K. EPSRC under Grant EP/T006951/1. (Xueyan Xing and Sainan Zhang contributed equally to this work.) (Corresponding authors: Hao Su; Yanan Li.)

This work involved human subjects or animals in its research. Approval of all ethical and experimental procedures and protocols was granted by Institutional Review Board at North Carolina State University under Application No. eIRB #24420, and performed in line with the NC State IRB Guidance.

Xueyan Xing and Yanan Li are with the Department of Engineering and Design, University of Sussex, BN1 9RH Brighton, U.K. (e-mail: y1557@sussex.ac.uk).

Sainan Zhang, Tzuhao Huang, Jin Sen Huang, and Hao Su are with the Lab of Biomechanics and Intelligent Robotics, Department of Mechanical and Aerospace Engineering, North Carolina State University, Raleigh, NC 27695 USA, also with the Joint NCSU/UNC Department of Biomedical Engineering, North Carolina State University, Raleigh, NC 27695 USA, and also with the University of North Carolina at Chapel Hill, Chapel Hill, NC 27695 USA (e-mail: hao.su796@ncsu.edu).

Color versions of one or more figures in this article are available at <https://doi.org/10.1109/TMECH.2024.3365045>.

Digital Object Identifier 10.1109/TMECH.2024.3365045

get nor meaningful due to the rapid changes of human–robot system properties when humans walk [5]. Adaptive control [13] is unable to overcome highly nonlinear uncertainties and disturbances with varying parameters, resulting in limited accuracy. A recent control strategy is time-based ILC, which can achieve the best accuracy among the aforementioned strategies [14], [15] thanks to its ability to handle periodical disturbance in time. Zhang and Steven [14] proposed an ILC to improve the ankle exoskeleton’s average and real-time torque tracking performance in steady-state walking by optimizing the parameters of ILC. Park et al. [15] designed a gait parameter adjustment method based on ILC for paraplegic wearers with powered exoskeletons. *However, ILC [14], [15] requires a fixed learning speed with a fixed iteration period, making unsteady-state walking difficult to handle, and is only suitable to handle periodic disturbance.* In addition to temporal periodicity, the motor control system of the exoskeleton has spatial periodicity due to the cyclic angle displacement according to the work in [16] and [17]. Therefore, the disturbance acting on the rotary motor of the exoskeleton can be generally regarded as joint-angle-related [18], [19]. In addition, reflex and intrinsic muscle stiffness and moment changes of human users are strongly spatially joint-angle-related [20] and an actuator with angle-related elasticity is accordingly proposed for a transfemoral prosthesis in [21]. As a result, in the presence of the aforementioned unsteady-state walking and joint-angle-related disturbance and system uncertainty, the ILC cannot guarantee high torque tracking accuracy and fast convergence, which motivates our spatial iterative learning (sIL) torque control.

This article aims to propose a sIL-based torque control for exoskeletons, where the high-level controller plans the reference torque requested by the user, the mid-level controller provides a position reference trajectory for the exoskeleton, and low-level controller ensures accurate tracking, respectively. The contributions of this article are as follows. 1) Our method can estimate and compensate for spatial uncertainties (e.g., joint-angle-related uncertain dynamics of the human–exoskeleton interaction system) and spatial disturbances (e.g., joint-angle-related disturbances caused by physical interaction with the human limb) that commonly exist in wearable robots to provide more accurate torque assistance to users with higher control accuracy. The advantages of our controller are due to its non-linearity and multilevels that allow spatial learning of joint-angle-related uncertainties and disturbances. This article has a different scope and contributions compared to the prior work of our group [2], which only focuses on exoskeleton mechatronics and high-level control design while this article focuses on developing a multilevel controller by involving a mid-level controller (which provides a trajectory for the exoskeleton to follow) and a low-level controller (which helps the human user achieve the reference assistive torque by trajectory tracking) for desired torque assistance. It also differs from the work in [22], which may need parameter estimation for disturbance learning. 2) Our method can handle unsteady-state walking and achieve highly accurate torque delivery with shorter convergence time by adapting to the unsteady-state gaits of different individuals. Thanks to its spatial learning capability that allows varying

learning speeds for different iterations, which is not allowed by ILC. To thoroughly verify the effectiveness of our method, we carried out two groups of experiments in terms of walking with fixed speed and changing gait to compare the state-of-the-art control strategies and our method.

## II. PROBLEM FORMULATION

### A. Preliminaries

This article uses the subscript  $s$  to represent the spatial function, and the variable without the subscript  $s$  can be regarded as time-related. For instance, we define a function  $\psi(t)$  and define the rotational displacement, i.e., the angle, in this article, as  $s$ . For  $t$  and  $s$ , there exists a mapping vector function  $\kappa$  satisfying  $s = \kappa(t)$  such that the spatial variable  $\psi_s(s)$  can be defined as  $\psi_s(s) = \psi_s(\kappa(t)) = \psi(t)$ . For the sake of simplicity, independent variables  $t$  for time-related functions and  $s$  for space-related functions are both neglected in this article. The subscript  $j, j = 1, 2, \dots, N$  denotes the iteration number during the control process.

### B. Dynamic Model of Human–Exoskeleton Interaction System

Before designing the controller, the human–exoskeleton interaction model was first formulated. Fig. 1(a) shows the exoskeleton platform we used in this article [2]. As illustrated in Fig. 1(b), the human–exoskeleton interaction system mainly comprises four components: 1) motor system, 2) gear reduction mechanism, 3) transmission mechanism, and 4) human lower limb.

The motor system can be modeled as

$$V - V_b = L\dot{i} + Ri \quad (1)$$

$$\tau_m = J_m\ddot{\theta}_m + b_m\dot{\theta}_m + \tau_b \quad (2)$$

$$k_i(i_r - i) = V, \tau_m = k_t i, V_b = k_b\dot{\theta}_m \quad (3)$$

where  $i_r$  is the reference current of the motor;  $i$  is the actual current of the motor;  $k_i$  is the resistance factor;  $V$  is the motor nominal voltage;  $V_b$  is the back-electromagnetic force;  $L$  is the motor inductance;  $R$  is the motor resistance;  $\tau_m$  is the torque generated by the motor related to the constant  $k_t$ ;  $k_b$  is the constant of  $V_b$ ;  $\theta_m$  is the motor rotation angle;  $J_m$  is the rotational inertia of the motor rotor;  $b_m$  is the damping coefficient;  $\tau_b$  is the output torque of the motor and it is also the input signal of the following gear reduction mechanism.

The dynamics of the gear reduction mechanism can be modeled as

$$\theta = \frac{\theta_m}{n}, \tau_g = n\tau_b \quad (4)$$

where  $n$  is the gear ratio;  $\tau_g$  is the output torque of the gearbox;  $\theta$  denotes the output rotation angle of the gearbox and it is also the joint angle of the interaction system.

The transmission section can be described as

$$\tau = \tau_g = k_c(\theta - \theta_h) = k_c\left(\frac{\theta_m}{n} - \theta_h\right) \quad (5)$$

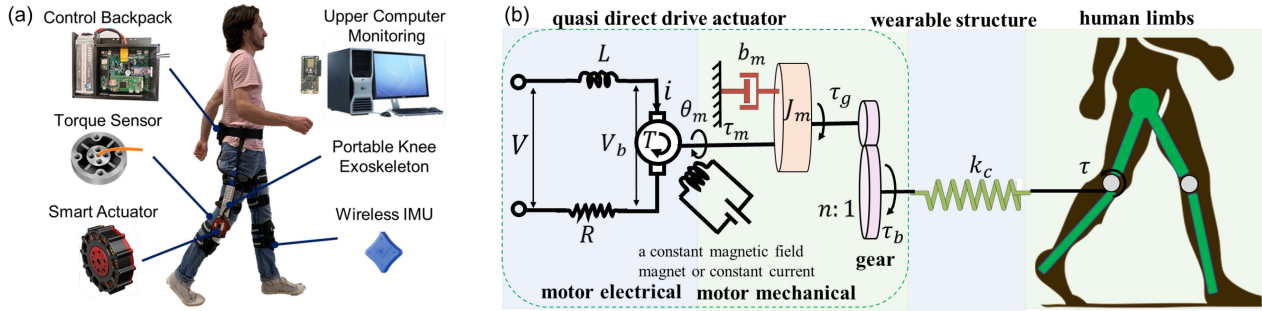


Fig. 1. Human-exoskeleton interaction system. (a) Overview of a portable knee exoskeleton. (b) Electromechanical components of knee exoskeleton.

where  $k_c$  is the coefficient representing transmission stiffness;  $\theta_h$  is the natural rotation angle of the human knee joint;  $\tau$  denotes the interaction torque exerted upon the lower limb of the human user.

Combing (2), (4), and (5), we have

$$\tau_m = J_m \ddot{\theta}_m + b_m \dot{\theta}_m + \frac{\tau}{n}. \quad (6)$$

Assuming the inductance  $L$  can be neglected due to its small value [23], using (1) and (3), we have

$$k_i(i_r - i) = Ri + k_b \dot{\theta}_m \quad (7)$$

which results in

$$\tau_m = \frac{k_t}{k_i + R} \left( k_i i_r - k_b \dot{\theta}_m \right) \quad (8)$$

where the torque generated by the motor  $\tau_m$  is expressed as a function of the reference current of the motor  $i_r$  and the motor rotation angle  $\theta_m$ .

Substituting (8) into (6), we have

$$\frac{J_m(R + k_i)}{k_i k_t} \ddot{\theta}_m + \frac{b_m(R + k_i) + k_t k_b}{k_i k_t} \dot{\theta}_m = i_r - \frac{R + k_i}{n k_i k_t} \tau \quad (9)$$

which reflects the relationship between  $\theta_m$ ,  $i_r$ , and the interaction torque  $\tau$ .

Substituting (4) into (9), the human-exoskeleton interaction model can be finally expressed as

$$m \ddot{\theta} + c \dot{\theta} = i_r - k \tau \quad (10)$$

where  $m = \frac{n J_m (R + k_i)}{k_i k_t}$ ,  $c = \frac{n b_m (R + k_i) + n k_t k_b}{k_i k_t}$ ,  $k = \frac{R + k_i}{n k_i k_t}$  are positive constants;  $\theta$  is regarded as the control state;  $i_r$  is the current control input to be designed.

In this article, the unknown factor  $d$ , including both angle-related disturbance and system uncertainty of the knee exoskeleton, is modeled as

$$d = \zeta_{cs} + \zeta_{ds} e + \zeta_{vs} \dot{e} \quad (11)$$

where  $\zeta_{cs}$ ,  $\zeta_{ds}$ , and  $\zeta_{vs}$  are angle-related and spatially periodic, which means  $\zeta_{cs,j} = \zeta_{cs,j-1}$ ,  $\zeta_{ds,j} = \zeta_{ds,j-1}$ ,  $\zeta_{vs,j} = \zeta_{vs,j-1}$  for the  $j$ th and  $(j-1)$ th gait cycles/iterations,  $e$  is the tracking error of the exoskeleton defined as  $e = \theta - \theta_r$ , where  $\theta_r$  is the reference trajectory of  $\theta$ , tracking which the desired assistive torque  $\tau_d$  can be achieved. Considering the modeled disturbance

in (11), the human-exoskeleton interaction model in (10) can be re-expressed as

$$m \ddot{\theta} + c \dot{\theta} = i_r + d - k \tau. \quad (12)$$

*Remark 1:* The space in sIL proposed in this article denotes the joint angular range of the human-exoskeleton interaction system. As mentioned in Section I, the term  $d$  in (11) contains undesirable effects caused by the system uncertainty and disturbance that are angle-related due to the periodicity of walking gaits. The disturbance due to physical interaction with the human limb is generally characterized by spatial periodicity since the changes in reflex and intrinsic muscle stiffness and moment of users during walking are both relevant to the angle of the interaction system due to the cyclic movement [20]. These types of disturbances depend on the joint angle of the interaction system  $\theta$ . The uncertain dynamics of the human-exoskeleton interaction model are also  $\theta$ -related due to the spatially periodic motor rotation of exoskeletons. As a result, it is expected to cancel the negative effects of spatial disturbance and uncertainty to ensure high control performance in terms of high tracking accuracy and short convergence time with the designed spatial learning hierarchy.

### III. SIL-BASED CONTROL DESIGN FOR KNEE EXOSKELETONS

In this section, we aim to propose a sIL-based strategy to achieve accurate walking assistance with a short convergence time. The control mechanism of the human-exoskeleton interaction system can be divided into high-, mid-, and low-level controllers, where the high-level one predetermines the desired torque required by the human user by collecting gait signals, and the middle-level one determines the reference trajectory of the human user. The low-level one controls the exoskeleton robot to let the interaction torque achieve the desired value for walking assistance. The block diagram of the structure of the human-exoskeleton system with the proposed control is illustrated in Fig. 2.

#### A. High-Level Controller

A high-level controller is needed to generate the desired torque. A human biomechanics model is used to estimate the biological knee moment during the gait cycle continuously. The



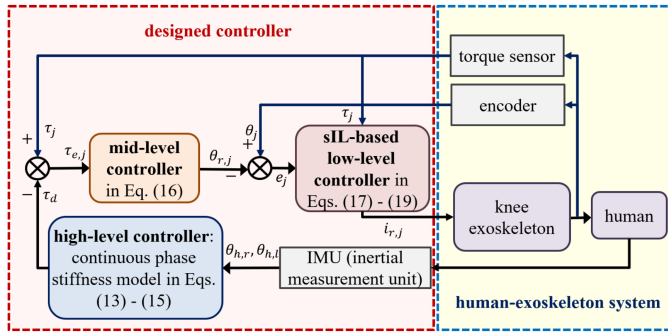


Fig. 2. Block diagram of the structure of the human-exoskeleton system with the proposed sIL-based interaction torque control algorithm. The high-level controller generates a reference torque profile based on the gait pattern. The mid-level controller provides a reference trajectory based on the interaction torque. The low-level controller achieves torque assistance based on sIL against changes and uncertainty.

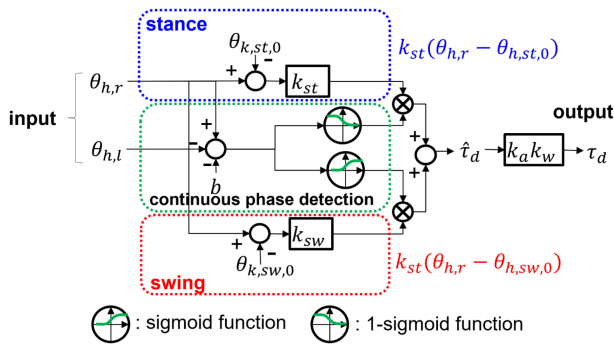


Fig. 3. High-level controller: Stiffness-based continuous torque controller with biological torque estimation. The inputs of the high-level control are the right knee angle and left knee angle. The output is the torque reference.

desired torque is used as the reference for the mid-level controller proportional to the estimated biological moment [2]. The knee joint transitions between high and low stiffness as the gait changes between the stance and swing phases, making the transition quasi-stiff. As shown in Fig. 3, only a few measurements (i.e.,  $\theta_{h,r}$  and  $\theta_{h,l}$  for right and left knee angle, respectively) in real time are needed to estimate the biological moment using a continuous phase stiffness model as the high-level controller. The detailed high-level controller scheme is shown in Fig. 3.

The high-level controller is adaptable to different individuals by the weight, which is given by

$$\tau_d = k_a k_w \hat{\tau}_d \quad (13)$$

where  $\tau_d$  is the reference torque that is generated by the high-level control,  $\hat{\tau}_d$  is the estimated biological knee moment that has been normalized,  $k_a$  is the assistive proportional gain, and  $k_w$  is the wearer's body mass (in kilogram). The torque reference estimation function (right leg) [2] is given by

$$\begin{aligned} \hat{\tau}_d = & [1 - S(\theta_{h,r}, \theta_{h,l})] K_{st} (\theta_{h,r} - \theta_{k,st,0}) \\ & + S(\theta_{h,r}, \theta_{h,l}) K_{sw} (\theta_{h,r} - \theta_{k,sw,0}) \end{aligned} \quad (14)$$

where  $K_{st}$  is the joint stiffness during the stance phase,  $K_{sw}$  is the joint stiffness during the swing phase,  $\theta_{k,st,0}$  is the equilibrium angle during the stance phase of the stiffness model,  $\theta_{k,sw,0}$  is the equilibrium angle during the swing phase of the stiffness model, and  $S(\theta_{h,r}, \theta_{h,l})$  is the sigmoid function that generates a continuous value between 0 and 1, which is described as

$$S(\theta_{h,r}, \theta_{h,l}) = \frac{1}{1 + e^{-af(\theta_{h,r}, \theta_{h,l})}} \quad (15)$$

where parameter  $a$  controls the transition area's width. Thus,  $S(\theta_{h,r}, \theta_{h,l})$  is the probability of applying the swing phase model while  $[1 - S(\theta_{h,r}, \theta_{h,l})]$  is the probability of applying the stance phase. The estimated optimal hyperplane  $f(\theta_{h,r}, \theta_{h,l})$  is given by  $f(\theta_{h,r}, \theta_{h,l}) = (\theta_{h,r} - \theta_{h,l}) - b$ , where  $b$  controls the center of the transition area. Finding the optimal transition between the stance and swing phase is complex yet crucial, so we used nonlinear optimization methods to identify the optimal hyperplanes to separate the two gait phases as  $\min \sum_{i=1}^m (\hat{\tau}_d - \tau_d)^2$ . This optimizer is able to find the optimal parameters to segment stance and swing by minimizing the error between estimated torque and biological torque data.

## B. Mid-Level Controller

The mid-level controller aims to provide a reference trajectory to the knee exoskeleton. The torque error is defined as  $\tau_{e,j} = \tau_j - \tau_d$ , where  $\tau_j$  is the actual interaction torque in the  $j$ th iteration and measured by the loadcell and  $\tau_d$  is from the output signal of the high-level controller.

We define  $T_j$  as the actual time duration of the  $j$ th iteration satisfying  $T_j \in [0, T]$ , in which the constant  $T$  is the maximum iteration time duration, i.e., the maximum time of one walking step. The update law of the exoskeleton's reference trajectory  $\theta_{r,j}$  is then proposed as

$$\theta_{r,j} = \begin{cases} \theta_{r,j-1} - \lambda \tau_{e,j}, & \text{if } t \in [0, T_j] \\ \theta_{r,j-1}, & \text{if } t \in (T_j, T] \end{cases} \quad (16)$$

where  $\lambda$  is a positive constant.

*Remark 2:* The mid-level controller in (16) updates the reference trajectory of the exoskeleton based on the interaction force, and the update law is designed as a piecewise function to cancel the negative effects of the varying iteration periods caused by the varying walking speed of the user, which is motivated by the authors in [24] and [25].

## C. Low-Level Controller

The current control input of the knee exoskeleton in the  $j$ th iteration is designed as

$$i_{r,j} = i_{f,j} + i_{b,j} + i_{c,j} \quad (17)$$

where

$$\begin{aligned} i_{f,j} &= m\ddot{\theta}_{r,j} + c\dot{\theta}_{r,j} + k\tau_j \\ i_{b,j} &= ce_j - k_e e_j - k_v \dot{e}_j \\ i_{c,j} &= -\hat{c}_{d,j} - \hat{c}_{d,j} e_j - \hat{c}_{v,j} \dot{e}_j \end{aligned} \quad (18)$$

in which  $k_e$  and  $k_v$  are positive constants and the sIL laws are proposed as

$$\begin{aligned}\hat{\zeta}_{c,j} &= \begin{cases} \hat{\zeta}_{c,j-1} + \beta_c p_{v,j} \dot{e}_j, & \text{if } t \in [0, T_j] \\ \hat{\zeta}_{c,j-1}, & \text{if } t \in (T_j, T] \end{cases} \\ \hat{\zeta}_{d,j} &= \begin{cases} \hat{\zeta}_{d,j-1} + \beta_d p_{v,j} \dot{e}_j e_j, & \text{if } t \in [0, T_j] \\ \hat{\zeta}_{d,j-1}, & \text{if } t \in (T_j, T] \end{cases} \\ \hat{\zeta}_{v,j} &= \begin{cases} \hat{\zeta}_{v,j-1} + \beta_v p_{v,j} \dot{e}_j^2, & \text{if } t \in [0, T_j] \\ \hat{\zeta}_{v,j-1}, & \text{if } t \in (T_j, T] \end{cases} \end{aligned} \quad (19)$$

where  $\beta_c$ ,  $\beta_d$ , and  $\beta_v$  are positive constants,  $p_{v,j} = |v_j|^{-1}$  is a time-varying function with  $v_j$  being the current angular velocity of the knee exoskeleton, and the iteration period  $T_j$  allows to be variable in different iterations.

#### D. Stability Proof

The following theorem showing the stability of our proposed multilevel interaction force controller for knee exoskeleton robots is introduced.

*Theorem 1:* With our proposed control strategy [high-level controller in (13), (14), mid-level in (16), low-level in (17)–(19)], the knee exoskeleton can help the human user achieve a desired interaction torque, i.e.,  $\lim_{j \rightarrow \infty} \tau_j = \tau_d$  and  $\lim_{j \rightarrow \infty} \tau_{e,j} = 0$  can be realized in the presence of spatial disturbance and system uncertainty.

*Proof:* Similar to (5), the desired assistive torque, which is independent of the iteration number, can be expressed as  $\tau_d = k_c(\theta_d - \theta_h)$  for analysis, where  $\theta_d$  is a desired trajectory provided to the human user by the knee exoskeleton, tracking which  $\tau_d$  can be obtained. Notice that  $\theta_d$  and  $\theta_h$  are irrelevant to the iteration number due to the inherent dynamic characteristics of individuals, which means the proposed control strategy is suitable for different individuals with sIL.

With (5),  $\tau_{e,j}$  can be expressed as

$$\tau_{e,j} = k_c(\theta_j - \theta_h) - k_c(\theta_d - \theta_h) = k_c e_{d,j} \quad (20)$$

where  $e_{d,j} = \theta_j - \theta_d$ .

In (18),  $i_{c,j}$  can be re-expressed as

$$i_{c,j} = -\hat{\zeta}_{cs,j} - \hat{\zeta}_{ds,j} e_j - \hat{\zeta}_{vs,j} \dot{e}_j \quad (21)$$

where  $\hat{\zeta}_{cs,j}$ ,  $\hat{\zeta}_{ds,j}$ , and  $\hat{\zeta}_{vs,j}$  are spacial forms of  $\hat{\zeta}_{c,j}$ ,  $\hat{\zeta}_{d,j}$ , and  $\hat{\zeta}_{v,j}$ , respectively.

For the  $j$ th iteration, substituting (17) and (18) into (12) achieves

$$m\ddot{e}_j + k_v \dot{e}_j + k_e e_j = \tilde{\zeta}_{cs,j} + \tilde{\zeta}_{ds,j} e_j + \tilde{\zeta}_{vs,j} \dot{e}_j \quad (22)$$

where  $\tilde{\zeta}_{cs,j} = \zeta_{cs,j} - \hat{\zeta}_{cs,j}$ ,  $\tilde{\zeta}_{ds,j} = \zeta_{ds,j} - \hat{\zeta}_{ds,j}$ , and  $\tilde{\zeta}_{vs,j} = \zeta_{vs,j} - \hat{\zeta}_{vs,j}$ .

##### 1) Proving the Effectiveness of the Low-Level Controller:

To verify when  $j \rightarrow \infty$ ,  $\theta_j = \theta_{r,j}$ , we define the system Lyapunov function as  $J_{p,j} = J_{e,j} + J_{c,j} + J_{d,j} + J_{v,j}$ , where

$$\begin{aligned} J_{e,j} &= \frac{1}{2}(m\dot{e}_j^2 + k_e \bar{e}_j^2), & J_{c,j} &= \frac{1}{2\beta_c} \int_0^s \tilde{\zeta}_{cs,j}^2(\eta) \operatorname{sgn}(v_{s,j}) d\eta, \\ J_{d,j} &= \frac{1}{2\beta_d} \int_0^s \tilde{\zeta}_{ds,j}^2(\eta) \operatorname{sgn}(v_{s,j}) d\eta, & J_{v,j} &= \frac{1}{2\beta_v} \int_0^s \tilde{\zeta}_{vs,j}^2(\eta) \\ & \operatorname{sgn}(v_{s,j}) d\eta, \text{ where } t \in [0, T), \bar{e}_j = \begin{cases} e_j, & \text{if } t \in [0, T_j] \\ e_j(T_j), & \text{if } t \in (T_j, T] \end{cases}, \end{aligned}$$

and  $\operatorname{sgn}(\cdot)$  is a sign function.  $J_{c,j}$  can be rewritten as  $J_{c,j} = \frac{1}{2\beta_c} \int_0^t \tilde{\zeta}_{cs,j}^2(\omega) |v_j(\omega)| d\omega > 0$ , which indicates its positiveness. Similarly, we have  $J_{d,j} > 0$  and  $J_{v,j} > 0$ . As a result, the Lyapunov function  $J_{p,j}$  is positively defined on the time domain. The derivative of  $J_{e,j}$  with respect to time is  $\dot{J}_{e,j} = \dot{e}_j(\bar{m}\dot{e}_j + \bar{k}_e e_j)$ , where  $\bar{m}$  and  $\bar{k}_e$  are two positive constants whose definitions will be given in the following.

Define  $\Delta J_{e,j} = J_{e,j} - J_{e,j-1}$ ,  $\Delta J_{c,j} = J_{c,j} - J_{c,j-1}$ ,  $\Delta J_{d,j} = J_{d,j} - J_{d,j-1}$ ,  $\Delta J_{v,j} = J_{v,j} - J_{v,j-1}$ , and then, Case i of  $t \leq T_j$  and Case ii of  $T_j < t \leq T$  are considered.

*Case i:*  $t \leq T_j$ . In this case,  $\bar{m} = m$  and  $\bar{k}_e = k_e$ . Substituting (22) into  $\dot{J}_{e,j}$ , it obtains

$$\dot{J}_{e,j} = \dot{e}_j \left( \tilde{\zeta}_{cs,j} + \tilde{\zeta}_{ds,j} e_j + \tilde{\zeta}_{vs,j} \dot{e}_j - k_v \dot{e}_j \right) \quad (23)$$

where  $\tilde{\zeta}_{c,j} = \zeta_{c,j} - \hat{\zeta}_{c,j}$ ,  $\tilde{\zeta}_{d,j} = \zeta_{d,j} - \hat{\zeta}_{d,j}$ ,  $\tilde{\zeta}_{v,j} = \zeta_{v,j} - \hat{\zeta}_{v,j}$ , and  $\zeta_{c,j}$ ,  $\zeta_{d,j}$ ,  $\zeta_{v,j}$  are the temporal formal of  $\zeta_{cs}$ ,  $\zeta_{ds}$ , and  $\zeta_{vs}$ , respectively.

Integrating  $\dot{J}_{e,j}$  from 0 to  $t$ , it generates

$$\begin{aligned} J_{e,j} &= \int_0^t \dot{e}_j(\omega) \left( \tilde{\zeta}_{c,j}(\omega) + \tilde{\zeta}_{d,j}(\omega) e_j(\omega) \right. \\ & \left. + \tilde{\zeta}_{v,j}(\omega) \dot{e}_j(\omega) - k_v \dot{e}_j(\omega) \right) d\omega. \end{aligned} \quad (24)$$

Since  $J_{e,j-1} > 0$ , we have

$$\begin{aligned} \Delta J_{e,j} &\leq \int_0^t \dot{e}_j(\omega) \left( \tilde{\zeta}_{c,j}(\omega) + \tilde{\zeta}_{d,j}(\omega) e_j(\omega) \right. \\ & \left. + \tilde{\zeta}_{v,j}(\omega) \dot{e}_j(\omega) - k_v \dot{e}_j(\omega) \right) d\omega. \end{aligned} \quad (25)$$

Define  $\Delta \hat{\zeta}_{cs,j}(\eta) = \hat{\zeta}_{cs,j}(\eta) - \hat{\zeta}_{cs,j-1}(\eta)$ , and then, we have  $\tilde{\zeta}_{cs,j}(\eta) - \tilde{\zeta}_{cs,j-1}(\eta) = -\Delta \hat{\zeta}_{cs,j}(\eta)$ .

According to the definition of  $J_{c,j}$ , it obtains

$$\begin{aligned} \Delta J_{c,j} &= \frac{1}{2\beta_c} \int_0^s \left( \tilde{\zeta}_{cs,j}^2(\eta) \operatorname{sgn}(v_{s,j}) \right. \\ & - \tilde{\zeta}_{cs,j}(\eta) \tilde{\zeta}_{cs,j-1}(\eta) \operatorname{sgn}(v_{s,j}) \\ & + \tilde{\zeta}_{cs,j}(\eta) \tilde{\zeta}_{cs,j-1}(\eta) \operatorname{sgn}(v_{s,j}) - \tilde{\zeta}_{cs,j-1}^2(\eta) \operatorname{sgn}(v_{s,j}) \\ & \left. + \tilde{\zeta}_{cs,j-1}^2(\eta) \operatorname{sgn}(v_{s,j}) - \tilde{\zeta}_{cs,j-1}^2(\eta) \operatorname{sgn}(v_{s,j-1}) \right) d\eta \end{aligned}$$

which leads to

$$\begin{aligned} \Delta J_{c,j} &= -\frac{1}{\beta_c} \int_0^s \left( \tilde{\zeta}_{cs,j}(\eta) \operatorname{sgn}(v_{s,j}) \right. \\ & \left. + \frac{1}{2} \Delta \hat{\zeta}_{cs,j}(\eta) \operatorname{sgn}(v_{s,j}) \right) \Delta \hat{\zeta}_{cs,j}(\eta) d\eta \end{aligned} \quad (26)$$

so that we have

$$\Delta J_{c,j} \leq -\frac{1}{\beta_c} \int_0^t \tilde{\zeta}_{c,j}(\omega) \Delta \hat{\zeta}_{c,j}(\omega) |v_j(\omega)| d\omega. \quad (27)$$

Similarly, we have  $\Delta J_{d,j} \leq -\frac{1}{\beta_d} \int_0^t \tilde{\zeta}_{d,j}(\omega) \Delta \hat{\zeta}_{d,j}(\omega) |v_j(\omega)| d\omega$  and  $\Delta J_{v,j} \leq -\frac{1}{\beta_v} \int_0^t \tilde{\zeta}_{v,j}(\omega) \Delta \hat{\zeta}_{v,j}(\omega) |v_j(\omega)| d\omega$ , where  $\Delta \hat{\zeta}_{d,j}(\omega) = \hat{\zeta}_{d,j}(\omega) - \hat{\zeta}_{d,j-1}(\omega)$  and  $\Delta \hat{\zeta}_{v,j}(\omega) = \hat{\zeta}_{v,j}(\omega) - \hat{\zeta}_{v,j-1}(\omega)$ .

Defining  $\Delta J_{p,j} = J_{p,j} - J_{p,j-1}$  and combining (25) and (27), we have

$$\begin{aligned} \Delta J_{p,j} &\leq \int_0^t \dot{e}_j(\omega) \left( \tilde{\zeta}_{c,j} + \tilde{\zeta}_{d,j} e_j(\omega) \right. \\ &\quad \left. + \tilde{\zeta}_{v,j} \dot{e}_j(\omega) - k_v \dot{e}_j(\omega) \right) d\omega \\ &\quad - \frac{1}{\beta_c} \int_0^t \tilde{\zeta}_{c,j}(\omega) \Delta \hat{\zeta}_{c,j}(\omega) |v_j(\omega)| d\omega \\ &\quad - \frac{1}{\beta_d} \int_0^t \tilde{\zeta}_{d,j}(\omega) \Delta \hat{\zeta}_{d,j}(\omega) |v_j(\omega)| d\omega \\ &\quad - \frac{1}{\beta_v} \int_0^t \tilde{\zeta}_{v,j}(\omega) \Delta \hat{\zeta}_{v,j}(\omega) |v_j(\omega)| d\omega. \end{aligned} \quad (28)$$

Using inequality (28) and (19), it obtains  $\Delta J_{p,j} = -k_v \int_0^t \dot{e}_j^2(\omega) d\omega \leq 0$ .

*Case ii:*  $T_j < t \leq T$ . For  $t \in (T_j, T]$ ,  $\bar{m}$  and  $\bar{k}_e$  are defined as  $\bar{m} = \bar{k}_e = 0$ , and  $\Delta \hat{\zeta}_{c,j}(\omega) = 0$ ,  $\Delta \hat{\zeta}_{d,j}(\omega) = 0$ ,  $\Delta \hat{\zeta}_{v,j}(\omega) = 0$  hold according to (19), and thus, we have  $\Delta J_{p,j} \leq -k_v \int_0^{T_j} \dot{e}_j^2(\omega) d\omega \leq 0$ .

Combining Cases i and ii, we have  $\lim_{j \rightarrow \infty} e_j = \lim_{j \rightarrow \infty} (\theta_j - \theta_{r,j}) = 0$ , which means that the knee exoskeleton can track its reference trajectory despite position-related disturbance.

**2) Verifying the Convergence of the Assistive Torque (The Effectiveness of the Mid-Level Controller):** Considering the updated law of the robot's reference trajectory, the system Lyapunov function is redefined as  $J_j = J_{p,j} + J_{f,j}$ , where  $J_{f,j} = \frac{k_c \lambda}{2} \int_0^t e_{d,j}^2(\omega) d\omega$  and  $\lambda$  is a positive constant.

To calculate  $\Delta J_{f,j}$ , Case 1 and Case 2 are reconsidered as follows.

*Case 1.*  $t \leq T_j$ : Define  $\Delta J_{f,j} = J_{f,j} - J_{f,j-1}$  and we have

$$\Delta J_{f,j} = \lambda k_c \int_0^t e_{d,j}(\omega) \Delta \theta_j(\omega) d\omega - \frac{\lambda k_c}{2} \int_0^t \Delta \theta_j^2(\omega) d\omega \quad (29)$$

where  $\Delta \theta_j(\omega) = \theta_j(\omega) - \theta_{j-1}(\omega)$ .

Since the tracking performance can be guaranteed under control in the sense of  $\lim_{j \rightarrow \infty} e_j = 0$ , when the iteration number is large enough,  $\Delta J_{f,j}$  can be rewritten as  $\Delta J_{f,j} \leq \lambda \int_0^t \tau_{e,j}(\omega) \Delta \theta_{r,j}(\omega) d\omega$ , where  $\Delta \theta_{r,j}(\omega) = \theta_{r,j}(\omega) - \theta_{r,j-1}(\omega)$ . Substituting (16) into (29), we have  $\Delta J_{f,j} \leq -\lambda \int_0^t \tau_{e,j}^2(\omega) d\omega < 0$ .

*Case 2.*  $T_j < t \leq T$ : From (16), it is known that the reference trajectory of the exoskeleton robot stops updating for  $t \in (T_j, T]$ , and then, in this case,  $\Delta J_{f,j} = J_{f,j} -$

---

### Algorithm 1: sIL-Based Multilevel Interaction Torque Control Design for Exoskeleton Robots.

---

**Input:**

Constant control coefficients  $\lambda, \beta_c, \beta_d, \beta_v, k_e, k_v$  and  $T$ ;

**Output:**

Current commands  $i_{f,j}, i_{b,j}, i_{c,j}$ ;

**1 begin**

2     Generate a desired assistive torque  $\tau_d$  based on gait pattern with Eqs. (13) and (14);

3     Initialization of learning variables  $\hat{\zeta}_{c,1}, \hat{\zeta}_{d,1}, \hat{\zeta}_{v,1}$ ;

4     **for**  $j = 1$  *to*  $N$  **do**

5         Compute the tracking force errors  $\tau_{e,j} = \tau_j - \tau_d$ ;

6         Compute the reference trajectory  $\theta_{r,j}$  using Eq. (16);

7         Compute the tracking error  $e_j = \theta_j - \theta_{r,j}$ ;

8         Compute current command  $i_{r,j}$  using Eqs. (17) and (18);

9         Send the current command  $i_{r,j}$  to robot actuators;

10         Update sIL laws  $\hat{\zeta}_{c,j+1}, \hat{\zeta}_{d,j+1}, \hat{\zeta}_{v,j+1}$  using Eq. (19);

11     **end**

**12 end**

---

$J_{f,j-1}$  can be rewritten as  $\Delta J_{f,j} \leq \lambda \int_0^{T_j} \tau_{e,j}(\omega) \Delta \theta_j(\omega) d\omega = -\lambda \int_0^{T_j} \tau_{e,j}^2(\omega) d\omega < 0$ .

Combining inequalities  $\Delta J_{p,j}, \Delta J_{f,j}$  for Case 1 and Case 2, we have  $\Delta J_j = \Delta J_{p,j} + \Delta J_{f,j} \leq 0$ . Then, if the initial energy of the system is bounded, we have  $\lim_{j \rightarrow \infty} J_j = 0$  and  $\lim_{j \rightarrow \infty} \tau_{e,j} = \lim_{j \rightarrow \infty} e_{d,j} = 0$ . As a result, the interaction torque tracking can be realized for the disturbed knee exoskeleton robot with uncertain dynamics under the proposed sILC scheme.

Unlike the low- and mid-level controllers that use tracking errors as control feedback, which may affect the system stability, the high-level controller uses the real-time measurement of bounded users' knee angles with sensors. As a result, our high-level controller is stable with bounded states with the help of sigmoid functions in (14) whose values vary between 0 and 1, i.e.,  $\tau_d \in L_\infty$ , as long as its parameters are set to be finite. The independent stabilities of high-level and mid- and low-level controllers contribute to the stability of the entire system [10].

### E. Implementation of Multilevel Controller for Exoskeletons

By observing (19), it is known that the sign of  $v_j$  should be invariant, i.e.,  $v_j > 0$  or  $v_j < 0$  holds, throughout the entire iterative process so that  $v_j$  never crosses zero to guarantee the existence of  $p_{v,j}$ . As a result, the sIL laws in (19) are only effective when the angular velocity direction of the exoskeleton does not change and when  $v_j$  is close to zero, the values of  $\hat{\zeta}_{c,j}, \hat{\zeta}_{d,j}$ , and  $\hat{\zeta}_{v,j}$  will increase with undesirable distortion. However, the whole process of knee movement is continuous with inevitable direction change. To solve this issue, the sIL laws in (19) are further improved as

$$\hat{\zeta}_{c,j} = \begin{cases} \hat{\zeta}_{c,j-1} + \beta_c \bar{v}_{v,j} \dot{e}_j, & \text{if } t \in [0, T_j] \\ \hat{\zeta}_{c,j-1}, & \text{if } t \in (T_j, T] \end{cases}$$

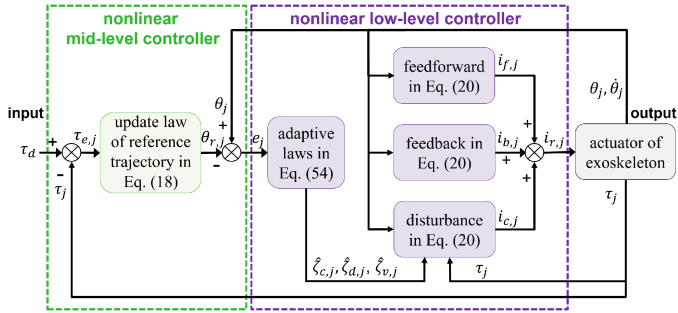


Fig. 4. Diagram of implementation of the sIL-based interaction torque control algorithm.

$$\hat{\zeta}_{d,j} = \begin{cases} \hat{\zeta}_{d,j-1} + \beta_d \bar{p}_{v,j} \dot{e}_j e_j, & \text{if } t \in [0, T_j] \\ \hat{\zeta}_{d,j-1}, & \text{if } t \in (T_j, T] \end{cases}$$

$$\hat{\zeta}_{v,j} = \begin{cases} \hat{\zeta}_{v,j-1} + \beta_v \bar{p}_{v,j} \dot{e}_j^2, & \text{if } t \in [0, T_j] \\ \hat{\zeta}_{v,j-1}, & \text{if } t \in (T_j, T] \end{cases} \quad (30)$$

where  $\bar{p}_{v,j} = \begin{cases} (|v_j| + \xi)^{-1} & \text{if } |v_j| < \gamma \\ |v_j|^{-1} & \text{if } |v_j| \geq \gamma \end{cases}$  and  $\xi$  and  $\gamma$  are user-defined positive constants.

Compared with (19), a constant  $\xi$  is added to (30) to help the sIL laws smoothly go through the phase during which  $v_j$  is close to zero. With the improved adaptive laws, the proposed sIL-based control scheme can smoothly switch between  $v_j < 0$  and  $v_j > 0$ , and thus, it is suitable for walking assistance of lower-limb movements. The final sIL-based control for the knee exoskeleton can be described by the designed high-level controller in (13) and (14), the mid-level in (16), and the improved low-level in (17), (18), and (30). The implementation of the proposed control strategy is illustrated in Fig. 4 and summarized in Algorithm 1. It is worth noting that our proposed multilevel robotic exoskeleton controller has good portability and can be applied to various types of exoskeleton robots, e.g., hip and upper-limb exoskeletons, by re-designing the high-level controller according to the exoskeleton type.

#### IV. SIMULATIONS

In this section, simulations are conducted to test the effectiveness of the proposed sIL-based control scheme.

The parameters of the exoskeleton robot are selected as  $n = 8 : 1$ ,  $R = 0.58 \Omega$ ,  $J_m = 8.95 \times 10^{-5} \text{kg} \cdot \text{m}^2$ ,  $k_t = 0.288 \text{N} \cdot \text{m}/\text{A}$ ,  $b_m = 0.08 \text{N} \cdot \text{m} \cdot \text{s}/\text{rad}$ ,  $k_i = 0.2 \Omega$ ,  $k_b = 0.2886 \text{V}/\text{kr}/\text{min}$ ,  $k_c = 10 \text{N} \cdot \text{m}/\text{rad}$ . A typical walking cycle of lower limbs is used to simulate the knee angle  $\theta_h$ . The desired interaction torque is designed as  $\tau_d = \sin(3\pi t) \text{N} \cdot \text{m}$  and the uncertain term  $d$  caused by the system uncertainty and angle-related disturbance is set as  $d = 8 \sin(2\pi\theta) + \theta e + 0.1\theta \dot{e} \text{N} \cdot \text{m}$ . The iteration number is designed to be  $N = 40$ . To notice,  $\tau_d$  is virtually designed only for simulation.

Parameters of the designed controller and adaptive laws are  $k_e = 20$ ,  $k_v = 0.2$ ,  $\beta_c = 2$ ,  $\beta_d = 1$ ,  $\beta_v = 0.4$ ,  $\xi = 1 \times 10^{-3}$ ,  $\gamma = 0.9$ , and  $\lambda = 0.05$ . The iteration period is set to be uncertain

between 0.9 s and 1 s to simulate the varying learning speed caused by the disturbance and uncertainty. The estimated speed disturbance in the  $j$ th iteration is designed as  $\hat{d}_j = \hat{\zeta}_{c,j} + \hat{\zeta}_{d,j} e + \hat{\zeta}_{v,j} \dot{e}$ .

The following three controllers are compared. First, combine the high-level control in (13)–(15) and the ILC method given by [10]

$$\theta_{r,j} = \beta \theta_{r,j-1} - K_I \tau_{e,j} \quad (31)$$

with  $\beta = 1$  and  $K_I = 0.05$ . Second, a typical PD control is used for tracking  $\theta_{r,j}$  in (31); and third, use the proposed sIL-based control scheme, i.e., sILC, in this article.

The output rotation angle of the gearbox  $\theta$  with PD and ILC is illustrated in Fig. 5(a). The actual limb–exoskeleton interaction torque in iterations of two cases is shown in Fig. 5(b). From Fig. 5(a) and (b), it is clear that the proposed sIL-based control strategy enables the lower limb to efficiently interact with the knee exoskeleton with the desired torque  $\tau_d$  after 20 iterations so that the assistance performance can be guaranteed even in the presence of the predefined disturbance and uncertainty. The learned and the actual disturbances in the last iteration are presented in Fig. 5(c). Observing Fig. 5(c), it is known that the term of undesirable effects  $d$  can be effectively learned by the proposed sIL laws in (30) by updating coefficients  $\hat{\zeta}_{c,j}$ ,  $\hat{\zeta}_{d,j}$ , and  $\hat{\zeta}_{v,j}$ , which demonstrates the availability of the sIL laws. As reflected in Fig. 5(a) and (b), the traditional ILC is subject to greater torque tracking error  $\tau_{e,j}$  compared with the proposed control due to the lack of learning and incapability of dealing with angle-related disturbance and uncertainty. Simulation results in Fig. 5 indicate that the proposed sIL-based control strategy is more stable and has better robustness. With its help, walking assistance is better served to the simulated human user with less assistive torque error.

#### V. EXPERIMENTS

Experiments were conducted to evaluate the proposed sIL-based control strategy's performance in a portable knee exoskeleton platform, which was presented in our previous work [2]. The experiment setup, as shown in Fig. 6, with the wearable robot consisting of a compact control electronic box, quasi-direct drive (QDD) actuators, loadcell sensors at each joint, two inertial measurement unit (IMU) sensors on each thigh, and wearable braces. We recruited three able-bodied subjects (subject #1: female, 1.6 m, 55 kg, 29 years old; subject #2: male, 1.74 m, 70 kg, 25 years old; subject #3: male, 1.80 m, 108 kg, 26 years old) to evaluate the performance of our proposed controller. The three subjects wore the powered knee exoskeleton and walked on a treadmill at steady-state walking (1.25 m/s) and varying-speed walking. The Institutional Review Board of North Carolina State University approved this experiment.

##### A. Interaction Torque for Walking Assistance

In this section, an experiment is conducted to test if the proposed sIL-based control strategy can stably generate a desired interaction torque between the human and knee exoskeleton



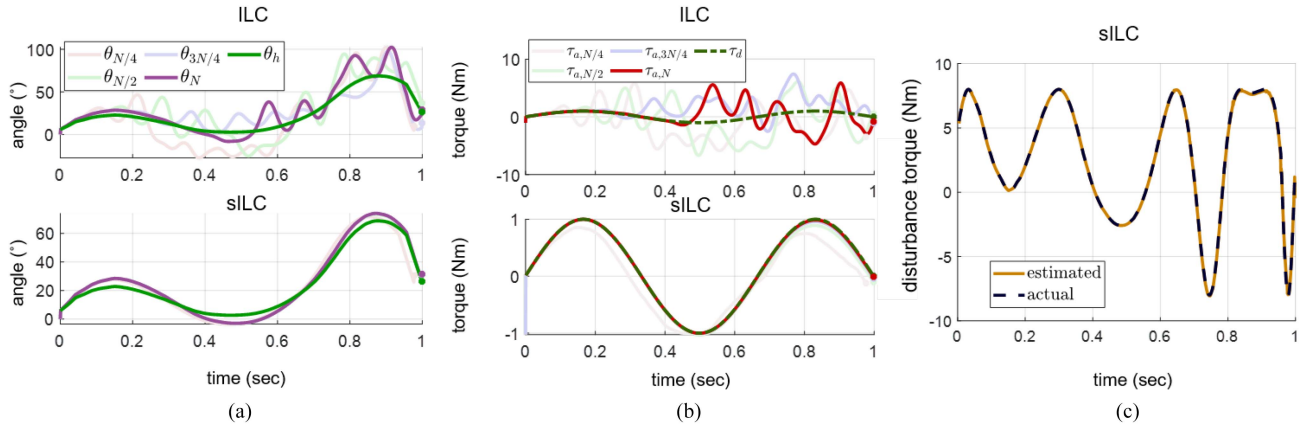


Fig. 5. Simulation results. (a) Output angle of the gearbox in iterations for ILC and proposed sILC. (b) Actual and desired interaction torques in iterations of ILC and proposed sILC. (c) Actual and estimated disturbances with proposed sILC.

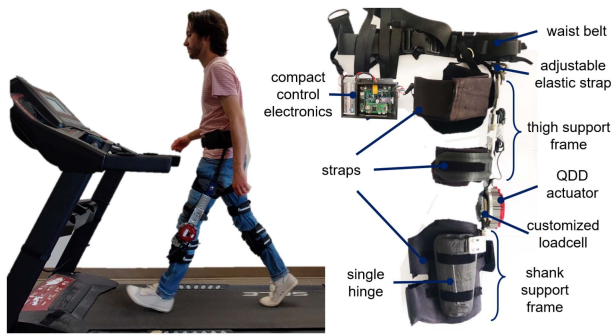


Fig. 6. Experiment setup. The left figure shows the subject walking on a treadmill. The right figure shows the structure of the knee exoskeleton. The exoskeleton consists of a compact control electronic box, a QDD actuator, a loadcell sensor, two IMU sensors, and a wearable structure that includes a waistband, adjustable elastic straps, a rigid thigh support frame, knee joint actuation system, and rigid shank support frame.

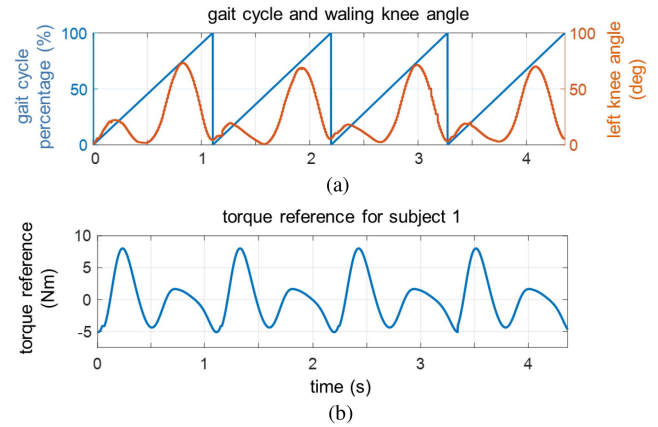


Fig. 7. (a) Measured left knee angle for continuous four strides, overlaid with gait cycle percentage. (b) Torque reference generated by the high-level controller in (13) and (14) for four continuous strides.

to realize walking assistance. Fig. 7 illustrates a walking example with the desired assistive torque profile generated by 1.25 m/s treadmill walking. The IMU sensors detected the human knee angles in real time, which were used to generate torque references based on high-level controllers (13) and (14). The desired output torque generated by the high-level controller, which is used for the middle- and low-level controllers, is illustrated in Fig. 7(b). Parameters of the designed controller and sIL laws are selected as  $K_{st} = 0.0379$ ,  $\theta_{k,st,0} = 5.322$ ,  $K_{sw} = 0.0046$ ,  $\theta_{k,sw,0} = 57.520$ ,  $a = 0.099$ ,  $b = 2.619$ ,  $k_e = 3$ ,  $k_v = 0.1$ ,  $\beta_c = 0.05$ ,  $\beta_d = 0.05$ ,  $\beta_v = 5 \times 10^{-4}$ ,  $\xi = 2 \times 10^{-5}$ ,  $\gamma = 6\pi/180$ , and  $\lambda = 0.0105$ . The iteration number is designed to be  $N = 100$ .

The learning results of (30) show the effects of the disturbance and the uncertainty to the knee exoskeleton. The learned coefficients of the disturbance, uncertainty, and overall values are displayed in Fig. 8. From Fig. 8(a), it is seen that  $\hat{\zeta}_{c,j}$ ,  $\hat{\zeta}_{d,j}$ , and  $\hat{\zeta}_{v,j}$  are dynamically regulated to learn the disturbance and uncertainty shown in Fig. 8(b), which is considerable and needs to be compensated in the control design.

### B. Steady-State Walking Comparison: sILC Is More Accurate, Faster, and Reduced More Metabolic Cost

To highlight the contributions of this article, we made experimental comparisons between our proposed sIL-based control strategy and existing control methods to observe their performances in walking assistance, including steady-state walking and varying walking speed experiments. The following three cases are considered.

Using the method in [2] with the following typical PID control, which is also called the noniterative method, as the low-level controller

$$\theta_r = -K_p \tau_e - K_I \int_0^t \tau_e(\xi) d\xi - K_D \frac{d\tau_e}{dt} \quad (32)$$

where  $K_p = 1$ ,  $K_I = 0.05$ , and  $K_D = 10^{-5}$ .

Using the traditional ILC method that is designed as (31) with  $\beta = 1$  and  $K_I = 0.0105$ .

Using the proposed sIL-based interaction force control, which is denoted as sILC in the following figures and analysis of experimental results.



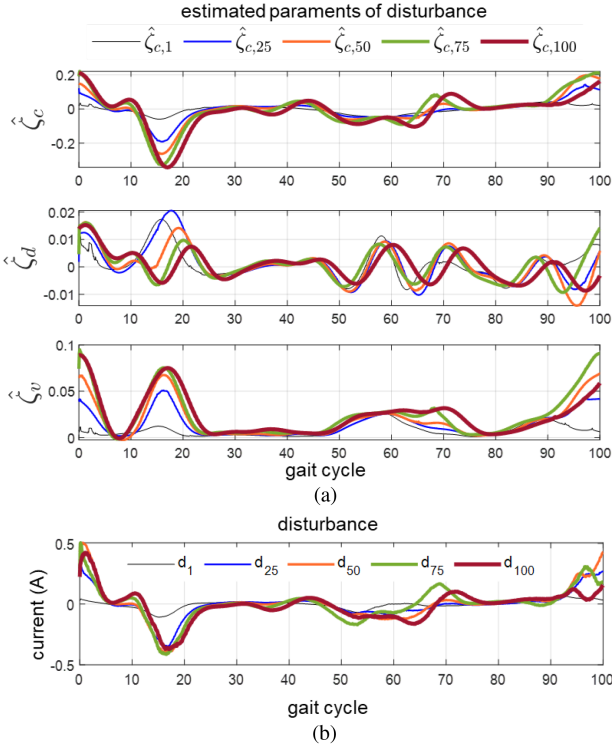


Fig. 8. (a) Learned coefficients of  $\hat{\zeta}_{c,j}$ ,  $\hat{\zeta}_{d,j}$ , and  $\hat{\zeta}_{v,j}$ . (b) Estimated disturbance in iterations.

In the steady-state walking experiment, the subjects are asked to walk 150 strides on the treadmill at 1.25 m/s for each case. Figs. 9 and 10 illustrate a single subject's (#1) detailed experimental cooperation results. Control performances, i.e., the torque tracking error for each gait cycle (or stride)  $\tau_{e,j}$ , are reflected in Fig. 9. From Fig. 9, it is known that the torque tracking error  $\tau_{e,N}$  with our proposed sILC strategy is smaller than the ones in the two other cases. To explore if the learning laws in our proposed control strategy can speed up the convergence, we compare the convergence speed of the proposed sILC method with the existing ILC method. Fig. 10 shows the desired and the actual torques in the 10th, 40th, and 80th iterations with ILC and sILC, respectively. Besides, their torque tracking root-mean-square (RMS) errors in different iterations are illustrated in Fig. 10(b). Observing Fig. 10(b), compared with sILC, which is convergent after the 80th iteration, the torque tracking error achieves its minimum value in the 80th iteration but increases again, which may be caused by the negative effects of the disturbance and uncertainty. As shown in Fig. 10, the proposed sILC strategy has better walking assistance performance with less torque error and has faster convergence due to its capability to deal with disturbance and uncertainty. Consequently, it outperforms the PID control and ILC in the sense of faster convergence and better assistance with less torque tracking error.

Due to the diversity of gaits and walking postures, the disturbance and uncertainty of walking differ for different individuals. Fig. 11 and Table I summarize the three subjects' test results

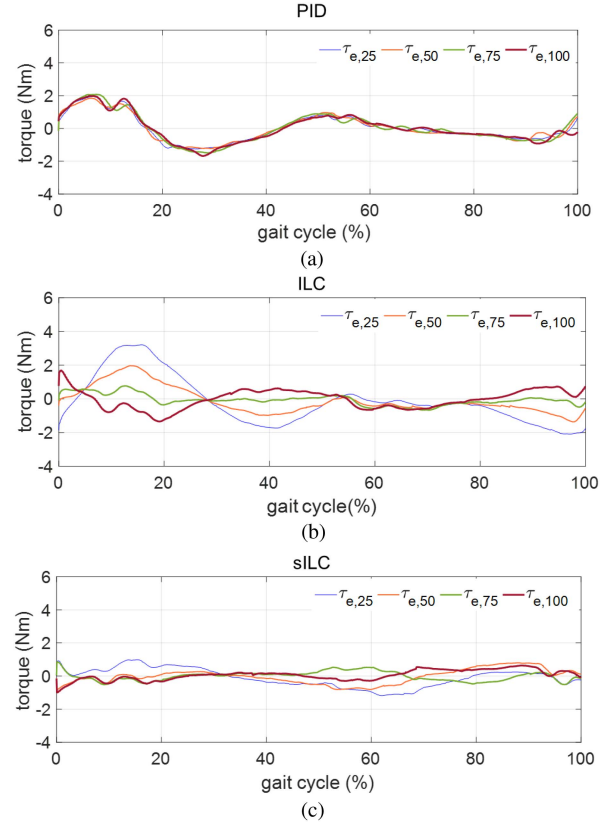


Fig. 9. Torque tracking error  $\tau_{e,j}$  ( $j = 25, 50, 75, 100$ ) in iterations with (a) PID control, (b) ILC, and (c) sILC.

TABLE I  
COMPARISON OF THREE METHODS UNDER STEADY-STATE WALKING

		Iteration number	Convergence time	Net metabolic change	Torque tracking error
PID	Subject 1	-	black -	4.64%	13.7%
	Subject 2	-	-	5.56%	11.8%
	Subject 3	-	-	-0.80%	11.7%
	Average	-	-	3.13%	12.4%
ILC	Subject 1	80	135.5 s	3.21%	5.2%
	Subject 2	77	125.5 s	6.54%	6.8%
	Subject 3	75	131.8 s	-1.07%	8.6%
	Average	77.3	130.9 s	2.89%	6.9%
sILC	Subject 1	40	72.2 s	-1.55%	3.4%
	Subject 2	41	65.4 s	2.94%	3.1%
	Subject 3	40	61.8 s	-3.20%	3.2%
	Average	40.3	66.5 s	-0.60%	3.2%

regarding torque tracking error, iteration number, convergence time, and metabolic changes in three cases to verify the generality of our proposed sILC method. The torque error percentage is calculated by rms errors of the first stride after convergence over the peak torque of desired torque  $\tau_{d,p}$ , where the RMS error is expressed as

$$\text{RMS error} = \frac{1}{\tau_{d,p}} \sqrt{\frac{1}{n} \sum_{i=1}^n (\tau_{j,i} - \tau_{d,i})^2} \times 100\% \quad (33)$$

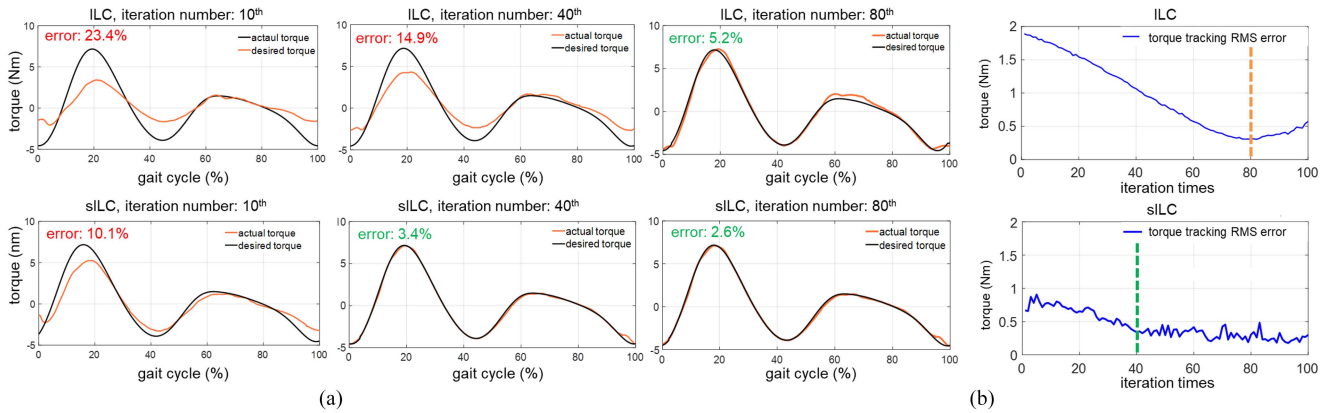


Fig. 10. (a) Desired and actual torques in the 10th, 40th, and 80th iterations of ILC and proposed sILC. (b) Torque tracking RMS errors in different iterations of ILC and proposed sILC. Our method completes the convergence 40 iterations while the ILC method needs 80 iterations. At the 80th iteration, the torque tracking error of our method sILC is only 2.6% while the error in the ILC is 5.2%.

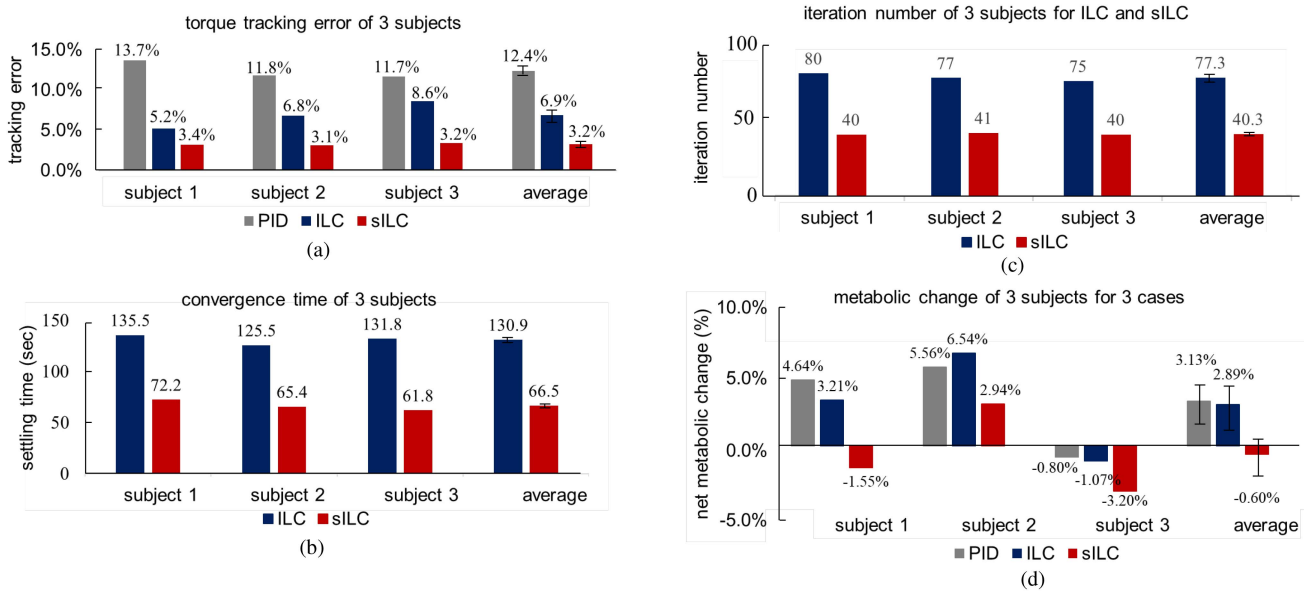


Fig. 11. (a) Torque tracking error and (b) iterations times of three subjects with three control methods, respectively. (c) Convergence time of three subjects with ILC and proposed control method. (d) Net metabolic (baseline versus powered condition changes of three subjects. On average, our sILC method achieved the lowest torque tracking error (3.2%), fastest convergence (iteration number: 40.3, convergence time: 66.5 s), and reduced 0.6% most metabolic cost.

in which  $j$  denotes the required iteration numbers to achieve control stability with ILC and proposed sILC that are displayed in Fig. 11(b). From Fig. 11(a), it is obvious that our proposed sILC can supply accurate torque walking assistance with less torque error and derivation. Fig. 11(b) demonstrates that our proposed method needs fewer iteration numbers than the ILC method. Fig. 11(c) compares the convergence times of the three subjects. Our proposed control method is 64.4 s faster than the existing methods and shortens the convergence time by nearly half (49.3%). Consequently, it has better and more stable performance as well as faster convergence because of its learning capability, and it can be applied to different individuals for effective walking assistance.

Unlike hip and ankle exoskeletons, consistent metabolic reduction in walking is more difficult for knee exoskeletons to

achieve since positive work done at the knee in level walking is less than that at the ankle or hip [2], [26]. In this metabolic test, subjects wore a respiratory measurement device (VO2 Master, Analyzer) and walked 5 min for each trial. Fig. 11(d) illustrates the net metabolic changes of three subjects. Compared with the baseline condition (not wearing the knee exoskeleton), the powered exoskeleton caused a 3.13% and 2.89% net metabolic increase with PID control and ILC, respectively, while our sILC strategy led to a 0.6% reduction in metabolic cost. These experimental results demonstrate our proposed control strategy's ability to reduce torque tracking error quickly and effectively since fewer iterations were required and the torque tracking error was the smallest of the three cases allowing the knee exoskeleton using our proposed strategy to provide more accurate and effective torque assistance to its wearer.

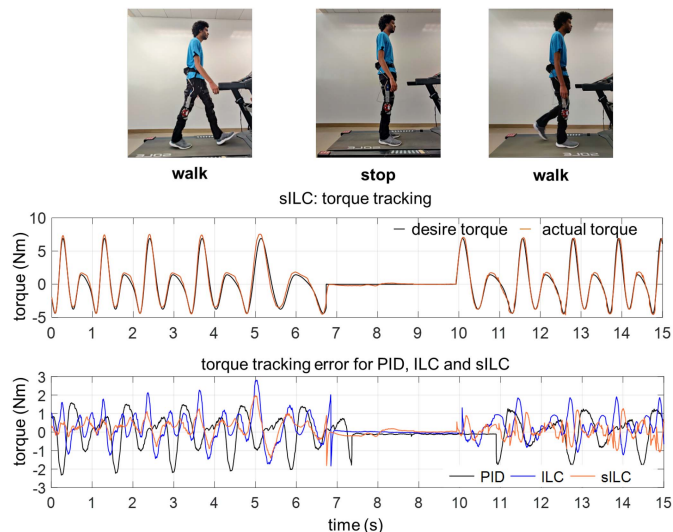


Fig. 12. Walk-stop-walk experiment. Torque tracking error percentage (rms error over peak torque) in the three methods are 13.9% (PID), 10.7% (ILC), and 6.8% (sILC), respectively.

### C. Varying-Speed Walking Comparison: Adaptive to Gait Pattern Changes and More Accurate

To understand the abilities of our proposed sIL-based control strategy to adapt to changes in gait patterns by spatially learning disturbance and uncertainty without requiring iteration periods to be the same, we conducted two different variable speed walking conditions tests. The first condition has the subject walk at 1.25 m/s for 100 s to allow the controller to learn the subject's normal gait pattern, then stop for a few seconds before walking again at 1.25 m/s to simulate sudden gait changes. Fig. 12 shows the error results within the last 14 s of this walking condition of our proposed sILC strategy compared to two existing control methods. The results showed our proposed sILC method to be more accurate than the other two methods. The RMS error and the percentage of peak torque for sILC were  $0.5 \text{ N} \cdot \text{m}$  and 6.8%, respectively, which was smaller compared to PID's  $1.0 \text{ N} \cdot \text{m}$  and 13.9% and ILC's  $0.7 \text{ N} \cdot \text{m}$  and 10.7%.

Three subjects participated in the second experiment with variable walking speed, which also included three different control methods, with each test lasting for 350 s. In the first 100 s, each subject walked on the treadmill at a uniform speed of 1.5 m/s. In the last 250 s, the subject's walking speed slowed from 1.5 to 0.5 m/s before increasing to 1.5 m/s again. This acceleration and deceleration process was repeated three times. Fig. 13 and Table II show the detailed experimental comparison results. Fig. 13 illustrates the torque tracking error under varying walking speeds for three subjects. Our sILC had the lowest torque tracking error compared to the other control methods. Table I quantifies the variable speed testing results, which shows that the PID control had the highest average percentage error to the peak of 10.39% while the ILC method and sILC method had average percentage errors of 8.59% and 5.16%, respectively. Furthermore, our proposed method was able to converge faster with an average of 41 iterations with an average of 38.21 s

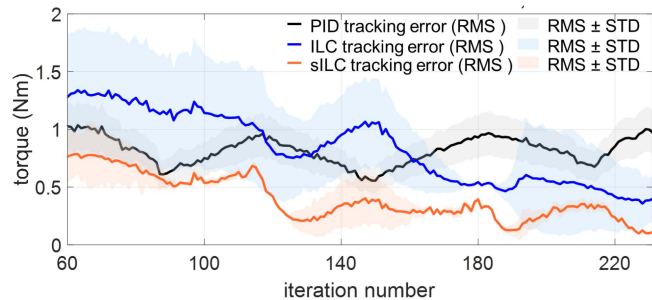


Fig. 13. Torque tracking error under varying walking speeds using three controllers. The experimental result showed that our sILC had the lowest torque tracking error among the three methods (PID: 10.39%, ILC: 8.59%, sILC: 5.16%).

TABLE II  
COMPARISON OF THREE METHODS UNDER VARYING WALKING SPEEDS

		iteration number	convergence time	average tracking RMSE (after convergence)	percentage of peak torque
PID	Subject 1	-	-	0.71 N·m	10.30%
	Subject 2	-	-	0.8458 N·m	10.42%
	Subject 3	-	-	1.0463 N·m	10.45%
ILC	Subject 1	112	115.62 s	0.55 N·m	7.69%
	Subject 2	106	105.78 s	0.66 N·m	8.40%
	Subject 3	117	122.85 s	0.97 N·m	9.70%
sILC	Subject 1	39	36.32 s	0.41 N·m	5.77%
	Subject 2	34	31.69 s	0.42 N·m	5.40%
	Subject 3	50	46.62 s	0.43 N·m	4.3%

convergence time compared to the ILC method's average of 112 iterations and 114.75 s convergence time. The results from both the walk-stop-walk test and variable speed test demonstrate our proposed sILC method's ability to respond quickly to changes in gait patterns while maintaining low-torque tracking errors.

## VI. CONCLUSION

This article proposes a sIL-based interaction torque control strategy for robotic exoskeletons. Due to its spatial learning of spatial (joint-angle-related) disturbances and system uncertainties, the interactive torque between user limbs and exoskeletons can iteratively achieve the desired value with high accuracy and a short convergence time for torque assistance. Compared to state-of-the-art control methods, it is also more adaptable to unsteady-state walking (e.g., sudden or gradual changes in gait speeds) of human users with less torque tracking error and faster convergence. The effectiveness of the proposed sIL-based control method is verified with simulation and experiment results. Although a knee exoskeleton is used as an example in this article, the proposed torque control method is applicable for various exoskeletons, e.g., hip exoskeletons, to provide effective motion assistance to users by properly modifying the low-level control according to the dynamics of the specific exoskeletons. Its use may also be extended to other scenarios of human-robot interaction [27], [28], [29], e.g., teleoperation, by removing the high-level controller that is specific for



exoskeleton robots to endow human users with stable performance in the presence of spatial disturbances and uncertainties caused by uncertain human behavior or environmental contact. In this article, a viscoelastic model is used for an approximation of the uncertainty and perturbation during exoskeleton control. However, for stochastic noises, e.g., measurement noises, this model may lose its efficacy. In future research work, we will focus on further improving the robustness of our designed controller when there are considerable noises in the system.

## REFERENCES

- [1] A. Bajpai et al., "Design and validation of a versatile high torque quasi-direct drive hip exoskeleton," *IEEE/ASME Trans. Mechatron.*, vol. 29, no. 1, pp. 789–797, 2024.
- [2] T.-H. Huang et al., "Modeling and stiffness-based continuous torque control of lightweight quasi-direct-drive knee exoskeletons for versatile walking assistance," *IEEE Trans. Robot.*, vol. 38, no. 3, pp. 1442–1459, Jun. 2022.
- [3] H. Zhu, C. Nesler, N. Divekar, V. Peddinti, and R. D. Gregg, "Design principles for compact, backdrivable actuation in partial-assist powered knee orthoses," *IEEE/ASME Trans. Mechatron.*, vol. 26, no. 6, pp. 3104–3115, Dec. 2021.
- [4] S. Galle, P. Malcolm, S. C. Hartley, and D. D. Clercq, "Reducing the metabolic cost of walking with an ankle exoskeleton: Interaction between actuation timing and power," *J. Neuroeng. Rehabil.*, vol. 14, no. 1, pp. 1–16, 2017.
- [5] Y. Ding, M. Kim, S. Kuindersma, and W. J. Conor, "Human-in-the-loop optimization of hip assistance with a soft exosuit during walking," *Sci. Robot.*, vol. 3, no. 15, 2018, Art. no. eaar5438.
- [6] G. S. Sawicki, B. D. Robertson, E. Azizi, and T. J. Roberts, "Timing matters: Tuning the mechanics of a muscle–tendon unit by adjusting stimulation phase during cyclic contractions," *J. Exp. Biol.*, vol. 218, no. 19, pp. 3150–3159, 2015.
- [7] Y. Sun, Y. Tang, J. Zheng, D. Dong, X. Chen, and L. Bai, "From sensing to control of lower limb exoskeleton: A systematic review," *Annu. Rev. Control*, vol. 53, pp. 83–96, 2022.
- [8] R. Gehlhar, M. Tucker, A. J. Young, and A. D. Ames, "A review of current state-of-the-art control methods for lower-limb powered prostheses," *Annu. Rev. Control*, vol. 55, pp. 142–164, 2023.
- [9] T. Yan, M. Cempini, C. O. Maria, and N. Vitiello, "Review of assistive strategies in powered lower-limb orthoses and exoskeletons," *Robot. Auton. Syst.*, vol. 64, pp. 120–136, 2015.
- [10] J. Zhang, C. C. Cheah, and S. H. Collins, "Experimental comparison of torque control methods on an ankle exoskeleton during human walking," in *Proc. IEEE Int. Conf. Robot. Automat.*, 2015, pp. 5584–5589.
- [11] H. Kazerooni and R. Steger, "The Berkeley lower extremity exoskeleton," *ASME J. Dyn. Sys., Meas., Control*, vol. 128, no. 1, pp. 14–25, Mar. 2006, doi: 10.1115/1.2168164.
- [12] A. Calanca, L. Capisani, and P. Fiorini, "Robust force control of series elastic actuators," *Actuators*, vol. 3, no. 3, pp. 182–204, 2014.
- [13] W. van Dijk, H. van der Kooij, B. Koopman, E. H. F. van Asseldonk, and H. van der Kooij, "Improving the transparency of a rehabilitation robot by exploiting the cyclic behaviour of walking," in *Proc. IEEE 13th Int. Conf. Rehabil. Robot.*, 2013, pp. 1–8.
- [14] J. Zhang and C. H. Steven, "The iterative learning gain that optimizes real-time torque tracking for ankle exoskeletons in human walking under gait variations," *Front. Neurobot.*, vol. 15, 2021, Art. no. 653409.
- [15] K.-W. Park, J. Choi, and K. Kong, "Iterative learning of human behavior for adaptive gait pattern adjustment of a powered exoskeleton," *IEEE Trans. Robot.*, vol. 38, no. 3, pp. 1395–1409, Jun. 2022.
- [16] C. Chen and Y. Yang, "Position-dependent disturbance rejection using spatial-based adaptive feedback linearization repetitive control," *Int. J. Robust Nonlinear Control: IFAC-Affiliated J.*, vol. 19, no. 12, pp. 1337–1363, 2009.
- [17] J. Xu and D. Huang, "Spatial periodic adaptive control for rotary machine systems," *IEEE Trans. Autom. Control*, vol. 53, no. 10, pp. 2402–2408, Nov. 2008.
- [18] I. V. Burkov and A. T. Zaremba, "Adaptive control for angle speed oscillations generated by periodic disturbances," in *Proc. 6th St. Petersburg Symp. Adaptive Syst. Theory*, 1999, pp. 34–36.
- [19] A. T. Zaremba, I. V. Burkov, and R. M. Stuntz, "Active damping of engine speed oscillations based on learning control," in *Proc. Amer. Control Conf.*, 1998, vol. 4, pp. 2143–2147.
- [20] M. M. Mirbagheri, L. Alibiglou, M. Thajchayapong, and W. Z. Rymer, "Muscle and reflex changes with varying joint angle in hemiparetic stroke," *J. Neuroengineering Rehabil.*, vol. 5, no. 1, pp. 1–15, 2008.
- [21] S. Pfeifer, A. Pagel, R. Riener, and H. Vallery, "Actuator with angle-dependent elasticity for biomimetic transfemoral prostheses," *IEEE/ASME Trans. Mechatron.*, vol. 20, no. 3, pp. 1384–1394, Jun. 2015.
- [22] J. Zhang, Y. Jiang, X. Li, H. Luo, S. Yin, and O. Kaynak, "Remaining useful life prediction of lithium-ion battery with adaptive noise estimation and capacity regeneration detection," *IEEE/ASME Trans. Mechatron.*, vol. 28, no. 2, pp. 632–643, Apr. 2023.
- [23] Y. Wang, A. Zahedi, Y. Zhao, and D. Zhang, "Extracting human-exoskeleton interaction torque for cable-driven upper-limb exoskeleton equipped with torque sensors," *IEEE/ASME Trans. Mechatron.*, vol. 27, no. 6, pp. 4269–4280, Dec. 2022.
- [24] D. Shen and J. Xu, "Adaptive learning control for nonlinear systems with randomly varying iteration lengths," *IEEE Trans. Neural Netw. Learn. Syst.*, vol. 30, no. 4, pp. 1119–1132, Apr. 2019.
- [25] Y. Li, X. Zhou, J. Zhong, and X. Li, "Robotic impedance learning for robot-assisted physical training," *Front. Robot. AI*, vol. 6, pp. 1–13, 2019.
- [26] G. S. Sawicki, O. N. Beck, I. Kang, and Y. J. Aaron, "The exoskeleton expansion: Improving walking and running economy," *J. Neuroeng. Rehabil.*, vol. 17, no. 1, pp. 1–9, 2020.
- [27] W. Qi and H. Su, "A cybertwin based multimodal network for ECG patterns monitoring using deep learning," *IEEE Trans. Ind. Inform.*, vol. 18, no. 10, pp. 6663–6670, Oct. 2022.
- [28] H. Su, W. Qi, J. Chen, and D. Zhang, "Fuzzy approximation-based task-space control of robot manipulators with remote center of motion constraint," *IEEE Trans. Fuzzy Syst.*, vol. 30, no. 6, pp. 1564–1573, Jun. 2022.
- [29] H. Su, W. Qi, Y. Schmirander, S. Ovrur, S. Cai, and X. Xiong, "A human activity-aware shared control solution for medical human–robot interaction," *Assem. Automat.*, vol. 42, pp. 388–394, 2022.



**Xueyan Xing** (Member, IEEE) received the B.S. degree in automation from Northeastern University, Shenyang, China, in 2015, the M.S. degree in control engineering from the Harbin Institute of Technology, Harbin, China, in 2017, and the Ph.D. degree in control theory and control engineering from Beihang University, Beijing, China, in 2020.

She was a Research Fellow with the Department of Engineering and Design, University of Sussex, Brighton, U.K., from 2020 to 2022. She was a Research Fellow with Continental-NTU Corporate Lab, Nanyang Technological University, Singapore, from 2022 to 2023. Her research interests include physical human–robot interaction, distributed control and optimization, distributed Nash equilibrium seeking, and vibration control.



**Sainan Zhang** received the M.S. degree in control science of engineering from the University of Electronic Science and Technology of China, Sichuan, China, in 2018, and the Ph.D. degree in mechanical engineering from the City University of New York, New York, NY, USA, in 2024.

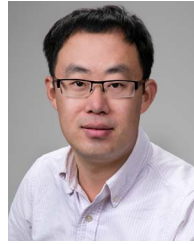
She is currently a Postdoctoral Fellow with the Department of Mechanical and Aerospace Engineering, North Carolina State University, Raleigh, NC, USA. Her current research interests include control, optimization, and design of wearable robots.





**Tzuhao Huang** received the B.S. degree in occupational therapy from National Cheng Kung University, Tainan, Taiwan, in 2004, the M.S. degree in rehabilitation from the Institute of Rehabilitation Science and Technology, National Yang Ming University, Taipei, Taiwan, in 2006, and the Ph.D. degree in mechanical engineering from National Taiwan University, Taipei, in 2013.

His current research interests include robotics, exoskeleton, rehabilitation, and machine learning.



**Hao Su** (Senior Member, IEEE) received the B.S. degree in automation from the Harbin Institute of Technology, Harbin, China, in 2006, the M.S. degree in mechanical engineering from the State University of New York University, Buffalo, NY, USA, in 2008, and the Ph.D. degree in mechanical engineering from Worcester Polytechnic Institute, Worcester, MA, USA, in 2013.

He is currently an Associate Professor with the Department of Mechanical and Aerospace Engineering, North Carolina State University, Raleigh, NC, USA, and also in the joint NCSU/UNC Biomedical Engineering Department, UNC Chapel Hill, Chapel Hill, NC. He was a Research Scientist with Philips Research North America and, then, a Postdoctoral Fellow with Harvard University and Wyss Institute for Biologically Inspired Engineering.

Prof. Su is a recipient of the National Science Foundation CAREER Award and Switzer Distinguished Fellowship of the U.S. Department of Health and Human Services. He is a Technical Editor of ASME/IEEE TRANSACTION ON MECHATRONICS, and an Associate Editor for IEEE ROBOTICS AND AUTOMATION MAGAZINE, IEEE ROBOTICS AND AUTOMATION LETTERS, IEEE International Conference on Robotics and Automation, and IEEE/RSJ International Conference on Intelligent Robots and Systems.



**Jin Sen Huang** received the Bachelor of Science and Master of Science degrees in mechanical engineering in 2018 and 2023, respectively, from North Carolina State University, Raleigh, NC, USA, where he is currently working toward the Ph.D. degree in mechanical engineering with the Department of Mechanical and Aerospace Engineering under the supervision of Dr. Hao Su.

His current research interest includes mechatronics design of wearable robots.



**Yanan Li** (Senior Member, IEEE) received the Ph.D. degree in robotics from the National University of Singapore, Singapore, in 2013.

From 2015 to 2017, he was a Research Associate with the Department of Bioengineering, Imperial College London, London, U.K. From 2013 to 2015, he was a Research Scientist with the Institute for Infocomm Research, Agency for Science, Technology and Research, Singapore. He is currently a Reader in robotics with the Department of Engineering and Design, University of Sussex, Sussex, U.K. His general research interests include human-robot interaction, robot control, and control theory and applications.